APPLIED SCIENCES AND ENGINEERING

# Soft, smart contact lenses with integrations of wireless circuits, glucose sensors, and displays

Jihun Park,[1]* Joohee Kim,[1]* So-Yun Kim,[1]* Woon Hyung Cheong,[1] Jiuk Jang,[1] Young-Geun Park,[1] Kyungmin Na,[2] Yun-Tae Kim,[3] Jun Hyuk Heo,[4] Chang Young Lee,[3] Jung Heon Lee,[4†] Franklin Bien,[2†] Jang-Ung Park[1†]



**Recent advances in wearable electronics combined with wireless communications are essential to the realization of medical applications through health monitoring technologies. For example, a smart contact lens, which is capable of monitoring the physiological information of the eye and tear fluid, could provide real-time, noninvasive medical diagnostics. However, previous reports concerning the smart contact lens have indicated that opaque and brittle components have been used to enable the operation of the electronic device, and this could block the user's vision and potentially damage the eye. In addition, the use of expensive and bulky equipment to measure signals from the contact lens sensors could interfere with the user's external activities. Thus, we report an unconventional approach for the fabrication of a soft, smart contact lens in which glucose sensors, wireless power transfer circuits, and display pixels to visualize sensing signals in real time are fully integrated using transparent and stretchable nanostructures. The integration of this display into the smart lens eliminates the need for additional, bulky measurement equipment. This soft, smart contact lens can be transparent, providing a clear view by matching the refractive indices of its locally patterned areas. The resulting soft, smart contact lens provides real-time, wireless operation, and there are in vivo tests to monitor the glucose concentration in tears (suitable for determining the fasting glucose level in the tears of diabetic patients) and, simultaneously, to provide sensing results through the contact lens display.**

## INTRODUCTION

Wearable electronic devices capable of real-time monitoring of the human body can provide new ways to manage the health status and performance of individuals (*1*–*7*). Stretchable and skin-like electronics, combined with wireless communications, enable noninvasive and comfortable physiological measurements by replacing the conventional methods that use penetrating needles, rigid circuit boards, terminal connections, and power supplies (*8*–*12*). Given this background, a smart contact lens is a promising example of a wearable, health monitoring device (*13*, *14*). The reliability and stability of soft contact lenses have been studied extensively, and significant advances have been made to minimize irritation of the eye to maximize the user's comfort. In addition, the user's tears can be collected in the contact lens by completely natural means, such as normal secretion and blinking, and used to assess various biomarkers found in the blood, such as glucose, cholesterol, sodium ions, and potassium ions (*13*). Thus, lens equipped with sensors can provide noninvasive methods to continuously detect metabolites in tears. Among various biomarkers, noninvasive detection of glucose levels for the diagnosis of diabetes has been studied in numerous ways to replace conventional invasive diagnostic tests (for example, finger pricking for drawing blood), as presented in table S1. By considering the correlation between the tear glucose level and blood glucose level (*15*), a glucose sensor fitted on a contact lens can provide the noninvasive monitoring of user's glucose levels from tear fluids with a consideration of the lag time between tear glucose level and blood glucose level in the range of 10 to 20 min (*13*–*16*).

Although such a system provides many capabilities, there are some crucial issues that must be addressed before practical uses of smart contact lens can be realized. These issues include (i) the use of opaque electronic materials for sensors, integrated circuit (IC) chips, metal antennas, and interconnects that can block users' vision (*15*, *17*, *18*); (ii) the integration of the components of the electronic device on flat and plastic substrates, resulting in buckled deformations when transformed into the curved shape for lenses, thereby creating foreign objects that can irritate users' eyes and eyelids (*19*); (iii) the brittle and rigid materials of the integrated electronic system, such as surface-mounted IC chips and rigid interconnects, which could damage the cornea or the eyelid (*20*–*22*); and (iv) the requirement for bulky and expensive equipment for signal measurements, which limits the use of smart contact lenses outside of research laboratories or clinical settings by restricting users' external activities (*14*, *15*, *20*, *23*).

For all of the reasons stated above, we have introduced an unconventional approach for the fabrication of a soft, smart contact lens where all of the electronic components are designed with normal usability in mind. For example, the wearer's view will not be obstructed because the contact lenses are made of transparent nanomaterials. In addition, these lenses provide superb reliability because they can undergo the mechanical deformations required to fit them into the soft lens without damage. The planar, mesh-like structures of the components of the device and their interconnects enable high stretchability for the curved soft lens with no buckling. In addition, display pixels integrated in the smart contact lens allow access to real-time sensing data to eliminate the need for additional measurement equipment.

To achieve these goals, we used three strategies, as described as follows: (i) For the design of soft contact lens, we formed soft contact lenses with highly transparent and stress-tunable hybrid structures, which are composed of mechanically reinforced islands to locate discrete electronic devices (such as rectifying circuits and display pixels) and elastic joints to locate a stretchable, transparent antenna and interconnect electrodes. The reinforced frames with small segments were

[1]School of Materials Science and Engineering, Ulsan National Institute of Science and Technology (UNIST), Ulsan 44919, Republic of Korea. [2]School of Electrical and Computer Engineering, UNIST, Ulsan 44919, Republic of Korea. [3]School of Life Sciences, School of Energy and Chemical Engineering, UNIST, Ulsan 44919, Republic of Korea. [4]School of Advanced Materials Science and Engineering, Sungkyunkwan University, Suwon 16419, Republic of Korea.
*These authors contributed equally to this work.
†Corresponding author. Email: jangung@unist.ac.kr (J.-U.P.); bien@unist.ac.kr (F.B.); jhlee7@skku.edu (J.H.L.)

made of a photo-patternable polymer, and the elastic parts were formed using a silicone elastomer, a conventional material for the soft contact lens. This contact lens based on the hybrid substrate, in which the reinforced islands were embedded inside an elastic layer, can effectively distribute the mechanical strain and protect ordinary electronics from mechanical deformations of the soft lens. Although the concept of using hybrid substrates for stretchable electronics has been reported previously, the use of hybrid substrates can degrade the optical properties of the resulting films significantly, leaving them with low transparency and high haze due to the difference in the refractive indices ($n$) of heterogeneous materials (*24*–*29*). Obviously, contact lenses should not obstruct the wearer's view, and they must have both high transparency and low haze for optical clarity. Thus, our hybrid substrate is composed of heterogeneous materials with negligible deviations in the refractive indices of the reinforced parts and the elastomer ($\Delta n$ = ~0.003). This index-matching approach can provide the wearer with a clear view, that is, outstanding transparency (93% in the visible light regime) and low haze (1.6% in the visible light regime). In addition, the elastic portion (conventional soft contact lens material) was maximized (more than 96.7%) in the total area of the contact lens for high oxygen permeability (Dk of 340.0 U). (ii) For the stretchable and transparent electrodes for antenna and interconnects, the electrodes for these passive components occupy relatively large areas of the final IC, so they must have high transparency and stretchability to be shaped into soft lens (*14*, *30*–*32*). Thus, one-dimensional (1D), ultralong metal nanofibers (mNFs) were directly electrospun as continuous networks to create transparent and stretchable electrodes (*33*). Charge transport occurs along these 1D metallic pathways, and their ultralong length facilitates the reduction of sheet resistance ($R_s$) by minimizing the number of junctions between the metal fibers. For example, random networks of these electrospun mNFs can present the wide ranges of superior $R_s$ and transparency (~1.3 ohm/sq with the transmittance of 90% or ~0.3 ohm/sq with the transmittance of 72% in the visible wavelength regime) by modulating the area fraction of mNFs. In addition, they also exhibit the outstanding stretchability (~30% in tensile strain), so they can be suitable as electrodes for interconnects in soft, smart contact lenses. In particular, their in-plane stretchability can prevent mechanical buckling of devices on a soft lens to delay the irritation of the eye or eyelid caused by feeling the presence of foreign objects. (iii) For wireless display pixels to visualize glucose levels in real time, after a graphene sensor detects the glucose concentration in the tears, the transparent and stretchable antenna with a rectifier drives the pixels of the light-emitting diode (LED) to display real-time sensing information wirelessly. For example, in this wireless circuit system, tear fluids with glucose concentration above the threshold will turn off the LED pixel. It is the first approach to apply the display pixel into a soft contact lens to visualize glucose sensing, which can be used to screen for prediabetes and monitor the glucose level daily, without the requirement of additional, bulky, and expensive measurement equipment.

In addition, wireless operations of this smart contact lens can maintain the eye temperature stably without abrupt heating, ensuring the safety of the wearer's eyes. Furthermore, in vivo tests using a live rabbit demonstrated its reliable operation without noticeable adverse effects. Therefore, this soft, smart contact lens provides a platform for wireless, continuous, and noninvasive monitoring of physiological conditions, as well as the detection of biomarkers associated with ocular and other diseases. In addition, it offers the potential for expanded applicability in other areas, such as smart devices for drug delivery and augmented reality.

## RESULTS

### Soft, smart contact lens system using stretchable and transparent devices

Figure 1A shows the layouts on the soft, smart contact lens where the glucose sensor, wireless power transfer circuit, and display pixel are fully integrated using transparent and stretchable interconnects. The main concept of this soft, smart contact lens system is the ability to monitor the status of the wearer's health wirelessly (that is, the glucose level in tears) through the LED pixel. For wireless operations, the transparent and stretchable inductive antenna and rectifier circuit were used in this system as the power transfer circuit. This power transfer circuit can wirelessly receive the power with ac signals using this antenna. The rectifier, which is composed of Si diodes and a capacitor, is integrated with the antenna to convert the ac signal into dc. More details about their fabrication steps are provided in the Supplementary Materials and Methods. The rectified dc power turns on the LED pixel and glucose sensor. Stress-tunable hybrid structures of the substrate (with mechanically reinforced islands and elastic joints) are used to protect these electronic devices from mechanical deformations of the soft lens. The rectifier circuit, glucose sensor, and LED pixel are located on the reinforced areas of this hybrid substrate. In addition, the stretchable antenna and interconnects are formed on the elastic regions, which are composed of a silicone elastomer, a commercial material for soft contact lenses. After the full integration with the glucose sensor and LED pixel, the transformation of the resulting sample with devices into the shape of a lens completes the fabrication of the soft, smart contact lens. More details of this fabrication procedure are presented in Materials and Methods and in movie S1.

Figure 1B shows the circuit diagram of the smart contact lens. In this smart lens, the antenna receives radio frequency (RF) signals from a transmitter (transmission distance, <9 mm), and the rectifier [combination of diode and capacitor (Cap.)] converts the ac signals into dc to turn on the LED and operate the sensor. The main mechanism of this contact lens to detect glucose levels is illustrated in Fig. 1C. Exposure to tear fluid with a glucose concentration above the threshold induces a reduction in the sensor resistance. This reduction in the sensor resistance decreases the resistance of the parallel circuit of the LED and sensor, whereas the resistance of other components (antenna and rectifier) in the system is constant. The bias applied to the parallel circuit of the LED and sensor reduces under the constantly applied voltage condition. This difference in the bias applied to the LED pixel can turn it on or off.

### Stretchable and transparent hybrid substrate

To use rigid electronic devices (for example, the LED pixel and rectifier circuit with Si diodes and a capacitor) in a stretchable system, the mechanical strain and fatigue applied on these devices should be relieved. For this purpose, a substrate was formed with the hybrid structure in which the mechanically reinforced islands are embedded inside a reversibly elastic layer. Figure 2A illustrates this hybrid substrate before or after stretching. For the fabrication of this hybrid substrate, the mechanically reinforced islands (OP) of a photocurable optical polymer (SPC-414; $E_{OP}$ = ~360 MPa) were photolithographically patterned with micrometer sizes (thickness, ~50 μm) on an 800-nm-thick Cu sacrificial layer. Then, the silicone elastomeric layer (LENS) of a soft contact lens material (elastofilcon A; $E_{LENS}$ = ~0.09 MPa) was coated successively to embed these reinforced parts with its thickness of ~100 μm. Eliminating the Cu sacrificial layer completed the formation of the hybrid substrate. More details about this fabrication procedure are provided in Materials and Methods and in fig. S1.

The capability to reduce the mechanical strain applied on these islands was confirmed by the stretching test of this hybrid substrate (Fig. 2, B and C). Although this hybrid film was stretched up to 30% in tensile strain, negligible strain (~0%) was applied on the reinforced islands, and the elastic region was mainly stretched because of the significant difference in Young's modulus (*24*, *27*, *28*). In addition, Fig. 2B shows that there were no gaps at the interfaces between these heterogeneous regions even during the stretching states (30% in tensile strain). Hence, these results indicate that our hybrid substrate system can offer sufficient stretchability over the entire region, whereas the brittle inorganic devices (LED, Si diode, and capacitor for the rectifier), which are located on the reinforced islands, can be protected from the mechanical deformations.

Figure 2D and fig. S2 present the atomic force microscopy (AFM) and scanning electron microscopy (SEM) images of the hybrid substrate with continuous interfaces between the reinforced and elastic areas. The

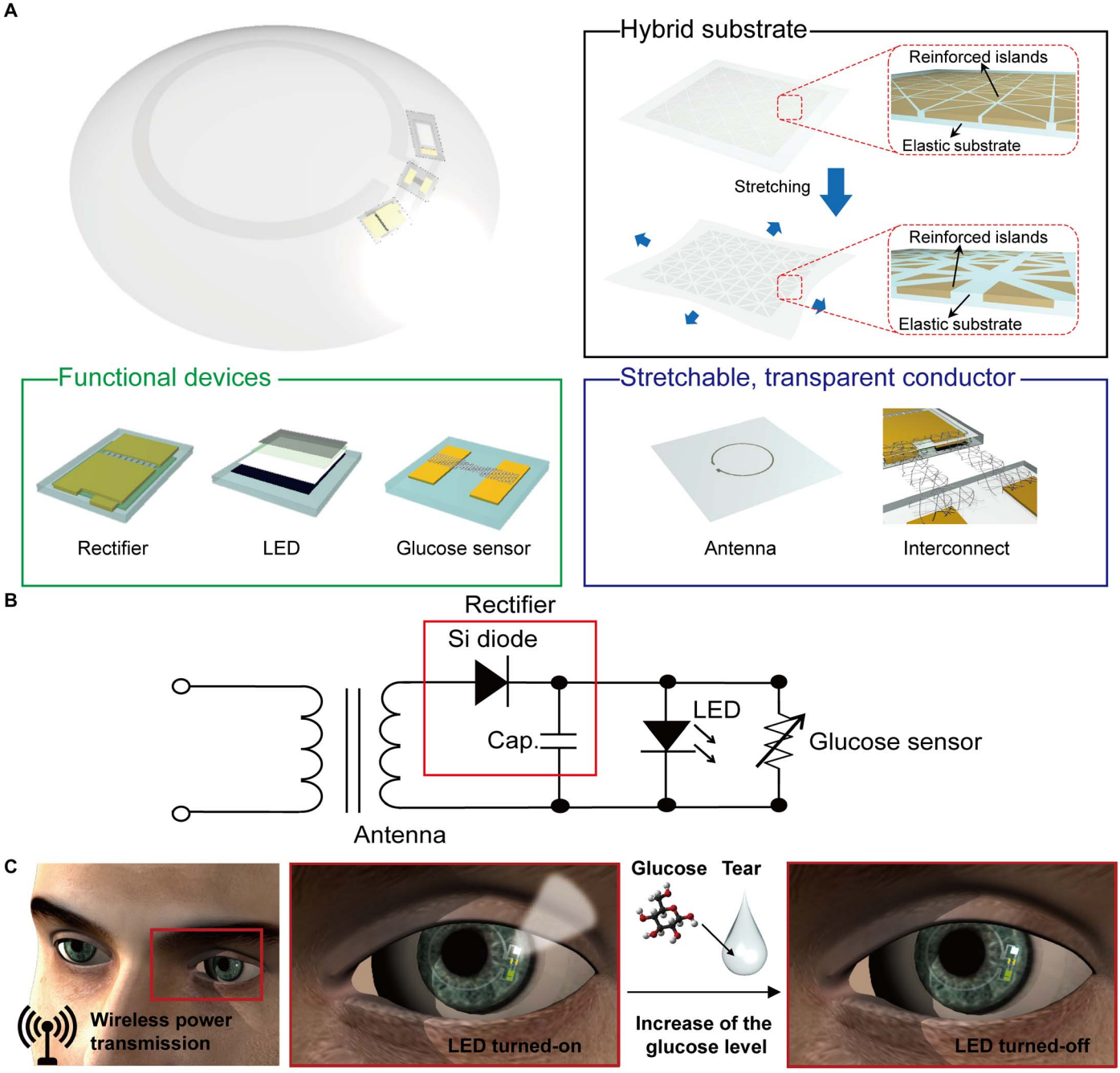


**Fig. 1. Stretchable, transparent smart contact lens system.** (**A**) Schematic illustration of the soft, smart contact lens. The soft, smart contact lens is composed of a hybrid substrate, functional devices (rectifier, LED, and glucose sensor), and a transparent, stretchable conductor (for antenna and interconnects). (**B**) Circuit diagram of the smart contact lens system. (**C**) Operation of this soft, smart contact lens. Electric power is wirelessly transmitted to the lens through the antenna. This power activates the LED pixel and the glucose sensor. After detecting the glucose level in tear fluid above the threshold, this pixel turns off.

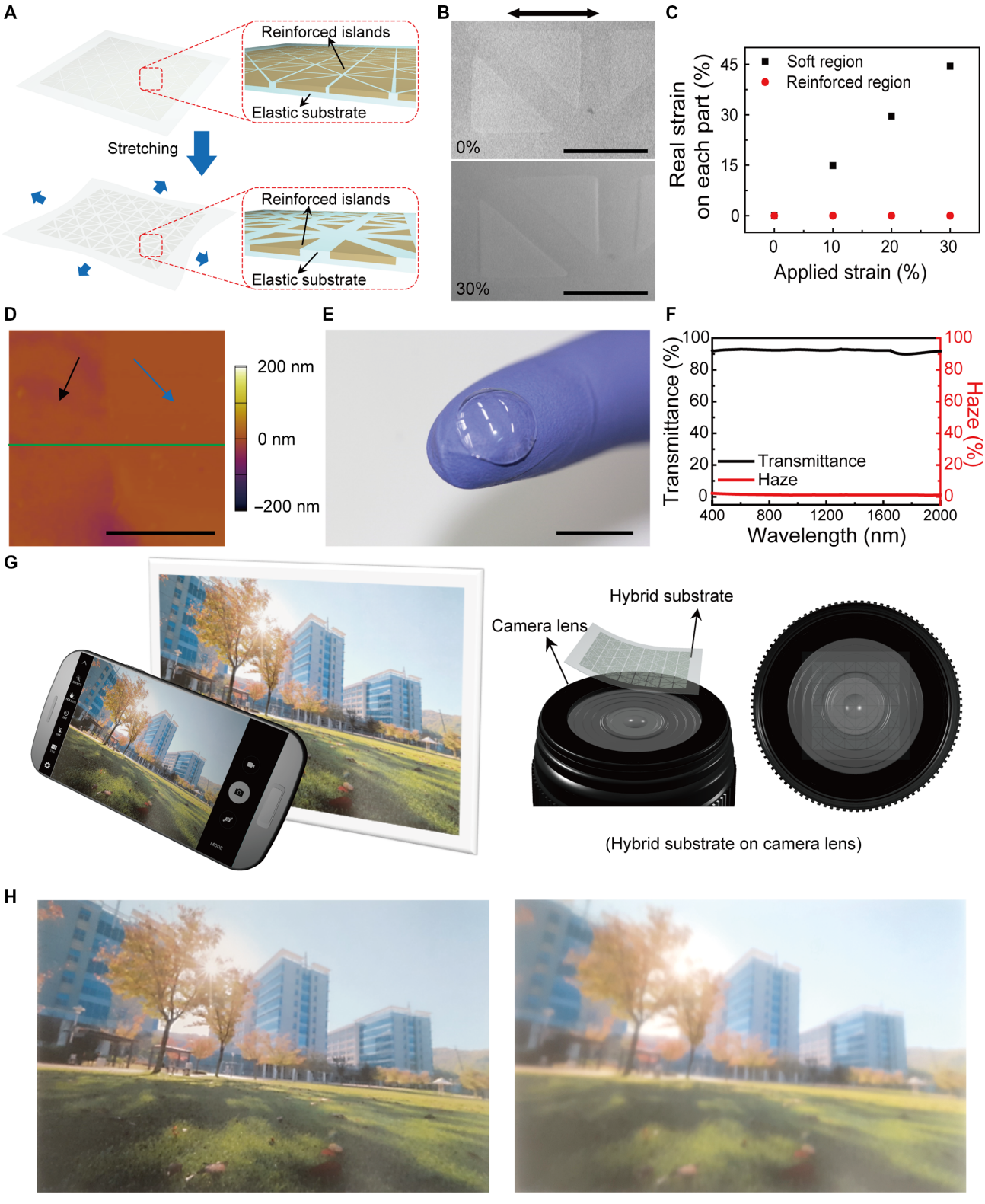


**Fig. 2. Properties of a stretchable and transparent hybrid substrate.** (**A**) Schematic image of the hybrid substrate where the reinforced islands are embedded in the elastic substrate. (**B**) SEM images before (top) and during (bottom) 30% stretching. The arrow indicates the direction of stretching direction. Scale bars, 500 μm. (**C**) Effective strains on each part along the stretching direction indicated in (B). (**D**) AFM image of the hybrid substrate. Black and blue arrows indicate the elastic region and the reinforced island, respectively. Scale bar, 5 μm. (**E**) Photograph of the hybrid substrates molded into contact lens shape. Scale bar, 1 cm. (**F**) Optical transmittance (black) and haze (red) spectra of the hybrid substrate. (**G**) Schematic diagram of the photographing method to identify the optical clarity of hybrid substrates. (**H**) Photographs taken by camera where the OP-LENS–based hybrid substrate (left) and the SU8-LENS–based hybrid substrate (right) are located on the camera lens.

root-mean-square (rms) surface roughness of the entire regime and the height difference at this interface were measured and found to be less than 3 and 5 nm, respectively. This nearly flat interface is advantageous in reducing light scattering from the interfacial surface, and it is in close contact with masks for photolithography. In addition, the optical characteristics of this hybrid film, such as its transparency and haze, are also important for its use as a contact lens. The difference in refractive indices of the reinforced islands and elastic parts can cause light scattering and decrease optical transparency by increasing the haze, which will disturb the wearer's vision (*34*). Therefore, the refractive indices of the silicone elastomer ($n = 1.41$) and the photocurable optical polymer for the reinforced patterns ($n = 1.407$) are similarly matched. As an example, Fig. 2E shows a photograph of a transparent contact lens produced using this hybrid film. This film (thickness, 100 μm) comprised the 6 × 6 array of the reinforced patterns (the pair of right-angled triangle shape, each of which measured 500 μm in length and 50 μm in thickness) with elastic space of 200 μm, and the elastomer part occupied ~40% of the entire area of the film. Figure 2F shows that this hybrid substrate exhibited superb optical transmittance (~93% at 550 nm) and low haze (~1.6% at 550 nm). This low haze value of the hybrid was similar to the case of a bare elastomer film with no heterogeneous part (~1.3% at 550 nm; fig. S3). In addition, the hybrid substrate preserved its transmittance and haze against its mechanical stretching (from 0 to 30% in tensile strain) (fig. S4).

To show the effect of refractive index on the wearer's vision, two different kinds of hybrid films were formed using the same silicone elastomer, that is, (i) one using OP as the reinforced parts and (ii) the other using SU8 epoxy polymer as the reinforced parts ($n = 1.595$). Then, after attaching these two different films onto the lens of a camera, photographs were made, as illustrated in Fig. 2G (an original photograph taken with no film is shown in fig. S5). Figure 2H demonstrates that the OP-LENS hybrid film ($\Delta n = 0.003$) provides a clearer image with lower haze than the SU8-LENS hybrid substrate ($\Delta n = 0.185$). This result means that the hybrid substrate with the well-matched refractive indices can prevent interference with the wearer's field of view.

## Characteristics of the wireless display on the hybrid substrate

The electrical and mechanical properties of the wireless display fabricated on a contact lens using the hybrid substrate were investigated, as shown in Fig. 3. This wireless display was composed of three electronic components (antenna, rectifier, and LED pixel), and these three parts were integrated and fabricated on an 800-nm-thick Cu sacrificial layer deposited on the Si wafer. After coating a 500-nm-thick parylene film on the Cu layer, the Si diodes and a $SiO_2$-based capacitor were connected in series as a rectifier circuit. Subsequently, the LED pixel was bonded using a silver epoxy glue. After the formation of the stretchable antenna and interconnects, the local patterns of the optical polymer (thickness, ~50 μm) selectively covered only the integrated form of the rectifier and LED and left the antenna and residual regions uncovered. After casting the silicone elastic layer (thickness, ~100 μm), removing the Cu sacrificial layer using wet etching, and flipping over the resulting film, the formation of the wireless display on the hybrid substrate was completed, where the rectifier and LED were embedded inside the reinforced region (OP) and the antenna and interconnects inside the elastic area (LENS), respectively. More details about the design and fabrication of the wireless circuit are described in figs. S6 and S7 and in Materials and Methods. Figure 3A illustrates the schematic layout of this wireless display.

Here, continuous networks of 1D, ultralong Ag nanofibers (AgNFs) were used as stretchable and transparent electrodes for the antenna and interconnects. A higher area fraction, which means higher density of AgNFs, can be formed by electrospinning for a longer period of time, and fig. S8A plots the $R_s$ and optical transmittance of these AgNF networks as a function of the area fraction. Both $R_s$ and transmittance decreased because their area fractions increased. AgNF networks with an area fraction of 0.2 had a low $R_s$ value of 0.3 ohm/sq (with transmittance of 72%). In addition, the AgNF networks exhibited good mechanical stretchability (with $\Delta R/R_0$ less than 10% under a tensile strain of 30%), as plotted in fig. S8B. Thus, this sample showed superior mechanical durability as a form of the antennas structure on curvilinear surfaces such as contact lenses. The AgNF networks (maximum thickness, 2 μm) were patterned for the antenna with a single-loop structure (diameter of antenna, 12 mm; width, 0.5 mm), as shown in Fig. 3A. This single-loop antenna of the smart lens, which can be located outside the pupil of a person's eye (diameter of pupil, ~6 mm), prevents interference with the wearer's field of view. Figure S8C presents the power transfer efficiency of this antenna measured at the distance of 5 mm from a transmitting coil, and the antenna most effectively absorbed RF energy at the frequency of 50 MHz, with a power transfer efficiency of 21.5%. In addition, the antenna received sufficient voltage (more than 10 V) to turn on LEDs wirelessly at 50 MHz (fig. S8D). Because of the outstanding stretchability of AgNF networks, the antenna inside the elastic region of the smart contact lens had a stable performance at 50 MHz with negligible degradation of power reception, even after mechanical stretching up to 30% in tensile strain (Fig. 3B).

For the conversion of the wirelessly transmitted ac bias to dc, a rectifier needs to be integrated into the antenna. The rectifier consisted of Si nanomembrane diodes connected with a capacitor in series, and the characteristics of the individual devices, with dimensions of 1.8 × 0.8 mm, are described in fig. S9. This rectifier was embedded inside the reinforced region of the lens and located outside the pupil where it would not interfere with the wearer's field of vision. Figure 3C shows that the Si diodes in this rectifier had a negligible change in their electrical performance even during the stretching state (30% in tensile strain) due to the hybrid substrate. This result proves that the hybrid substrate can protect ordinary electronics from mechanical fractures. In addition, the rectifier converts the ac signal at 50 MHz into a dc bias of 10 $V_{rms}$ (Fig. 3D).

The fabricated wireless display system, including the antenna, rectifier, and LED, using the hybrid substrate is stretchable, but it is flat, as shown in Fig. 3E. This flat and stretchable sample can be molded into a contact lens shape, as shown in fig. S10 and movie S1. Figure 3F shows the resulting soft contact lens (after molding) on an artificial eye. The resulting smart contact lens can receive inductively coupled ac power wirelessly from a transmitting coil (at 50 MHz) at the distance of 5 mm. Then, the transmitted ac signal can be rectified through the half-wave rectifying circuit to dc power to turn on the LED pixel (Fig. 3F and movie S2). Because the elastic area of the smart contact lens absorbs most of the applied strain, the integrated devices can operate reliably in the form of a soft contact lens.

## Glucose sensing with integrated smart contact lens

The wireless display was subsequently integrated with a glucose sensor to produce a soft, smart contact lens that can respond to the changes in glucose level and simultaneously display the sensing information through the LED pixel (Fig. 1C). The main mechanism of glucose sensing in this system is that for the selective and sensitive glucose

detection, glucose oxidase (GOD; β-D-glucose from *Aspergillus niger*) was immobilized on the graphene surface with a pyrene linker through the π-π stacking interaction (*35*, *36*). The part where GOD is linked to the pyrene by the amide bond was generated through the nucleophilic substitution reaction of *N*-hydroxysuccinimide (*36*). When glucose passes through the graphene channel of this sensor, it can be oxidized by GOD. After the oxidation, the reduced GOD can be oxidized again by reacting with oxygen molecules, which results in the formation of hydrogen peroxide as a by-product. This hydrogen peroxide is also decomposed, producing oxygen, protons ($H^+$ ion), and electrons (*14*, *16*, *37*). The protons cause the positive charge transfer effect of the graphene channel (p-type). The main reactions that occurred on the graphene channel are presented in fig. S11. Because the major carrier density is proportional to the glucose concentration, we can detect the relative change in resistance ($\Delta R/R_0$) of the sensor as a function of the glucose concentration generated from the above reaction processes (*14*, *38*). However, the continuous formation of $H_2O_2$ can degrade the enzymatic activity of GOD, lowering the sensitivity of this glucose sensor. Therefore, to remove $H_2O_2$ immediately, catalase (CAT), which can decompose $H_2O_2$ into $H_2O$ and $O_2$, was coimmobilized with GOD on the surface of the graphene channel (*39*). The use of CAT improved the sensitivity of the sensor by increasing the enzymatic activity of GOD (Fig. 4A). The average glucose levels of tears for normal people are in the range of 0.2 to 0.6 mM, but this average can exceed 0.9 mM for people with diabetes (*40*), and this sensor can detect these wide ranges (Fig. 4B). The relative change in resistance ($\Delta R/R_0$) of this sensor decreased linearly with the glucose concentration, as shown in the inset of Fig. 4B. The response time of the sensor is defined to be the time required for the sensor to reach 90% of the response. Therefore, the response time is measured as ~1.3 s, as shown in fig. S12. In addition, the sensitivity is defined as the slope of calibration curve (the inset of Fig. 4B), so the sensitivity is calculated as approximately −22.72%/mM. The measured signal-to-noise ratio (SNR) at 0.1 mM was 23.87, and the minimum detectable concentration (for the case of an SNR of ~3) was approximately estimated to be about 12.57 μM. Because human tears contain various species besides glucose, the selectivity of this sensor to glucose was tested using (i) a buffered solution and (ii) a solution of artificial tears. After adding glucose at the desired concentrations to



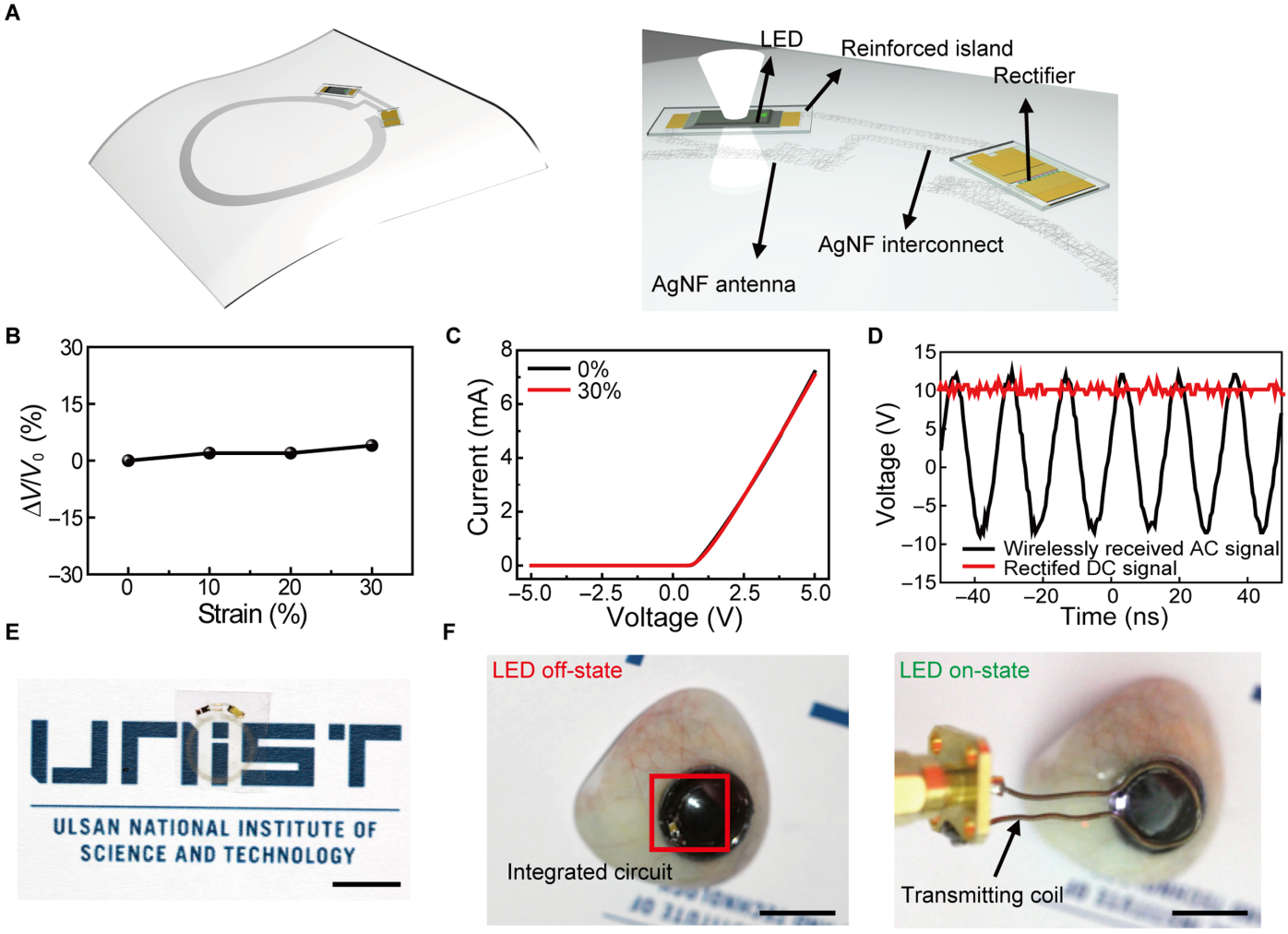


**Fig. 3. Wireless display circuit on the hybrid substrate.** (**A**) Schematic image of the wireless display circuit. The rectifier and LED are in the reinforced regions. The transparent, stretchable AgNF-based antenna and interconnects are in an elastic region. (**B**) Relative change in transmitted voltage by antenna as a function of applied strain. (**C**) Characteristics of Si diode on the hybrid substrate by applying 0 and 30% in tensile strain. (**D**) Rectified properties of the fabricated rectifier. (**E**) Photograph of wireless display on the hybrid substrate. Scale bar, 1 cm. (**F**) Photographs (left, off-state; right, on-state) of operating wireless display with lens shape located on the artificial eye. Scale bars, 1 cm.

these two solutions, the response ($\Delta R/R_0$) of this sensor was compared to these two cases. The deviation from the sensor response ($\Delta R/R_0$) was not significant for the cases of buffered or tear solutions, as shown in Fig. 4C, which indicates that other species in tears (besides glucose) had a negligible interference with this glucose sensor. In addition, the glucose sensor integrated on a soft contact lens was stretched, and its response was measured during the stretching. Figure 4D shows that the glucose sensor with the hybrid substrate has a negligible change in its resistance for a tensile strain of up to 30%, unlike the glucose sensor on a bare elastomeric film (with no use of the hybrid substrate). Despite the use of the soft lens, the location of this sensor on the reinforced part of the hybrid substrate prevents it from being damaged by mechanical deformations of the soft contact lens.

This glucose sensor was integrated with the wireless display (the LED pixel, rectifying circuit, and antenna) using the hybrid substrate as a fully functional smart contact lens. After fabricating the wireless display on the hybrid substrate, the Cu sacrificial layer was etched away to delaminate the sample. Subsequently, a parylene layer was partially etched to passivate the entire device region, except the channel part of the sensor to detect the glucose solution. The graphene channel was transferred onto this IC. Subsequently, these integrated components were embedded inside a soft contact lens using the molding process (movie S1). During this molding step, the graphene channel was open and locally uncovered by the lens material (silicone elastomer) for the physical contact of the channel with tears. Finally, GOD and CAT were immobilized on the surface of graphene to serve as a glucose sensor. Figure 5 (A and B) shows a schematic illustration and a photograph of the fully integrated contact lens, respectively. The AgNF-based electrodes and devices in the resulting smart contact lens are passivated by the parylene layer such that this passivation layer of parylene, as a diffusional barrier, prevents the leakage of AgNFs and simultaneously ensures the protection of the AgNFs from tear fluid (*41*). As presented in Fig. 5C, the resulting lens can prevent interference with the wearer's field of vision by placing the opaque components (LED and metal patterns) outside the human pupil and by matching the refractive indices of the reinforced material and the silicone elastomer with negligible deviation ($\Delta n$ = 0.003). The long-term stability of this smart lens was studied for repeatability during multiple usage by storing in an artificial tear solution for up to 48 hours. There is negligible degradation of the response even after 48 hours, which suggests that the enzymes maintain their activity for at least 48 hours (fig. S13A). In addition, this lens also showed nearly constant output voltages through the antenna-rectifier even after 48 hours because they are passivated by the hybrid substrate and parylene, which can act as a diffusional barrier (fig. S13B). Furthermore, its mechanical stability against the cyclic deformation was also investigated. After 5000 cycles of stretching and releasing with the tensile strain of 30%, the smart contact lens operated stably with negligible degradation (fig. S13C). Because the average glucose level of tears for fasting diabetic patients typically exceeds 0.9 mM and the concentration for fasting people without diabetes is below 0.6 mM (*39*), a glucose

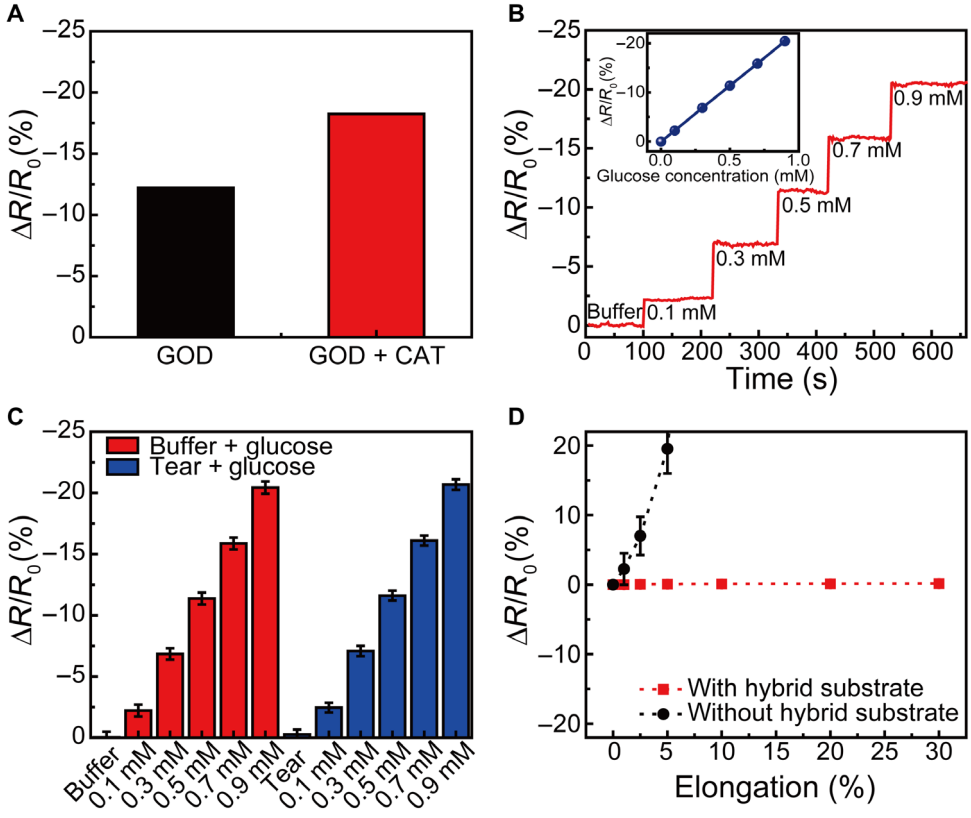


**Fig. 4. Characterization of the glucose sensor.** (**A**) Difference in response between glucose concentrations of 0.1 and 0.9 mM for the sensor with GOD functionalization (black) and GOD-CAT functionalization (red). (**B**) Real-time continuous monitoring according to the glucose concentrations (inset, calibration curves of the glucose sensor). (**C**) Electrical response for the sensors with different solutions (red, buffered solution; blue, solution of artificial tear). Each data point indicates the average for 10 samples, and error bars represent the SD. (**D**) Relative changes in the resistance of glucose sensor as a function of tensile strain (red, sensor on the hybrid substrate; black, sensor on the elastomeric film with no use of the hybrid substrate).

concentration of 0.9 mM was chosen in our circuit as the threshold to diagnose diabetes with the LED on/off indication. This threshold can be tuned simply by changing the resistance of the sensor. As the glucose concentration in tear fluid increases, the resistance of the sensor is reduced. This reduction in the sensor resistance decreases the resistance of the parallel circuit of the LED and sensor (Fig. 1B). However, the resistance of other components in this system is unchanged. This results in the reduction of the bias applied to the parallel circuit of the LED and sensor under the constantly applied voltage condition. Therefore, the bias applied to the LED pixel and the luminance of the LED decrease as the glucose concentration increases until the threshold (fig. S14). When the glucose concentration is above 0.9 mM, this pixel turns off because the bias applied to the LED becomes below than its turn-off voltage. Figure 5D shows a live rabbit wearing this smart contact lens for an in vivo test. After putting this soft lens onto the rabbit's eye, we were able to wirelessly monitor the increase of the glucose concentration above the threshold by observing the LED on/off operation. For the glucose concentration of more than 0.9 mM, the LED turned off, as shown in right image of Fig. 5D and movie S3. The rabbit showed no signs of abnormal behavior, and this smart lens remained stable during repeated eye blinks. The stable status of the smart contact lens was proven by the operations with higher power transfer (movie S3). The higher power induces the increase of current in the LED to turn it on, although the resistance of the sensor is reduced by glucose. Hence, the LED pixel turned off because the glucose concentration was over the threshold, not because of damage to the circuit. The design is such that the LED

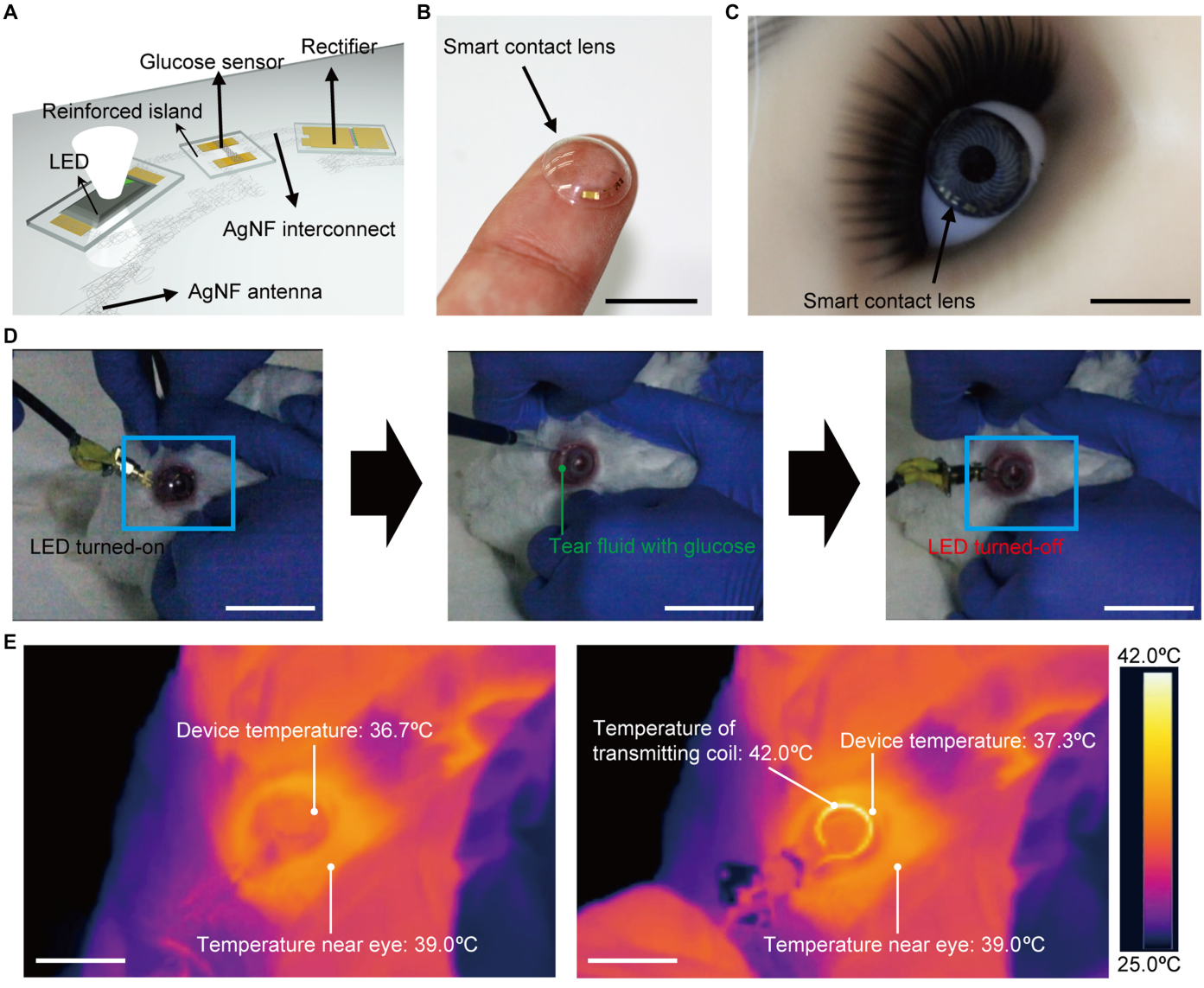


**Fig. 5. Soft, smart contact lens for detecting glucose.** (**A**) Schematic image of the soft, smart contact lens. The rectifier, the LED, and the glucose sensor are located on the reinforced regions. The transparent, stretchable AgNF-based antenna and interconnects are located on an elastic region. (**B**) Photograph of the fabricated soft, smart contact lens. Scale bar, 1 cm. (**C**) Photograph of the smart contact lens on an eye of a mannequin. Scale bar, 1 cm. (**D**) Photographs of the in vivo test on a live rabbit using the soft, smart contact lens. Left: Turn-on state of the LED in the soft, smart contact lens mounted on the rabbit's eye. Middle: Injection of tear fluids with the glucose concentration of 0.9 mM. Right: Turn-off state of the LED after detecting the increased glucose concentration. Scale bars, 1 cm. (**E**) Heat tests while a live rabbit is wearing the operating soft, smart contact lens. Scale bars, 1 cm.

turns off when the high glucose level is detected, which is counter-intuitive. Therefore, a design improvement for a smart lens system that provides an intuitive status to support usability represents a promising area for future work (for example, monitoring the level of biomarkers via a smartphone). Furthermore, the heat generation was monitored using an infrared camera during the wireless operation of this lens (Fig. 5E and movie S4). Although the rabbit was wearing the wirelessly operating lens circuit, the temperature of this lens device was maintained at ~37°C without any significant generation of heat. Although the wireless power transfer from the transmitting coil to the lens increased the temperature of this transmitting coil to ~42°C, which was slightly higher than the temperature of the surroundings, its wireless function prevented this coil from touching the rabbit's eye or eyelid with a gap of ~5 mm. Furthermore, according to simulation results for specific absorption rate (SAR) for a person, the maximum SAR value of our smart contact lens system was 1.399 W/kg (fig. S15), which is much lower than the regulation value (10 W/kg) (*42*).

## DISCUSSION

In conclusion, we developed a method to fabricate a soft, smart contact lens that can monitor glucose levels in tears to indicate the diabetic condition in real time through a display with wireless operations. For this smart lens, electronic components (that is, the glucose sensor, LED pixel, rectifier circuit, and the stretchable, transparent antenna) were integrated onto the mechanical stress-tunable hybrid substrate with well-matched refractive indices for high optical transparency and low haze. After molding this to the round shape of the soft contact lens, the integrated electronic system operated reliably during mechanical deformations, including bending and stretching. This rapid molding approach, together with conventional processing steps (for example, photolithography and metallization by evaporation), can represent its potential for large-scale mass production. The in vivo tests using a live rabbit, including the monitoring of the temperature change on the rabbit's eye, provided the substantial promise of future smart contact lenses for noninvasive health care monitoring using human eyes and tears.

## MATERIALS AND METHODS

### Preparation of the hybrid substrates

For the hybrid substrate, an 800-nm-thick Cu film was evaporated as a sacrificial layer on a Si wafer. Optical polymer (SPC-414, EFiRON) was spin-coated (1500 rpm for 30 s) for the thickness of 50 μm and photolithographically patterned as reinforced parts. Subsequently, an elastic polymer (elastofilcon A, CooperVision) mixing base and a curing agent with the ratio of 10:1 were also spin-coated (1000 rpm for 30 s) for the thickness of 100 μm and cured at 100°C for 1 hour. After that, the Cu sacrificial layer was etched by the diluted etching solution of $FeCl_3$/HCl/$H_2O$ [1:1:20 (v/v)] to delaminate the hybrid substrate from the Si wafer.

For the SU8-based hybrid substrate, SU8 3050 (MicroChem Corp.) was spin-coated (3000 rpm for 30 s) to a thickness of 50 μm and patterned as reinforced parts. The next steps were identical to the optical fiber polymer-based hybrid substrate.

### Embedding of the hybrid substrate or the IC in the contact lens

For the embedded structures, the hybrid substrate or the fabricated circuit on the hybrid substrate was placed within the mold for the contact lens. Subsequently, the contact lens material was fulfilled and thermally cured in 100°C for 1 hour, with pressing at 313 kPa. After curing, the hybrid substrate or IC embedded in the contact lens was detached from the mold.

### Fabrication of the wireless display on a smart contact lens

To assemble the stretchable and transparent antenna for wireless power transition, the AgNFs were simultaneously electrospun on the sample where the rectifier circuit was manufactured. Then, the electrospun AgNFs were patterned by photolithography and a wet etching process. After that, the LED pixel was bonded to the circuit by a silver epoxy glue. Subsequently, the hybrid substrate was manufactured on the sample, and then, the sacrificial layer was etched to delaminate the wireless display. The molding process for the contact lens shape was identical with the embedding of the hybrid substrate or the IC in the contact lens.

### Fabrication of glucose sensor

For the characterization of the glucose sensor, on a Si wafer with a 300-nm-thick thermal oxide layer (for electrical measurements), Cr/Au (3:100 nm), which served as source and drain, was evaporated and patterned by photolithography. Subsequently, a graphene layer synthesized by chemical vapor deposition (CVD) was transferred onto the sample and patterned by photolithography to form the channel (width, 300 μm; length, 500 μm) simultaneously. Then, the SU8 layer was patterned to open only channel regions to functionalize the graphene channel. To immobilize GOD and CAT on the graphene channel for the efficient detection of glucose, the fabricated sensor was placed in 1-pyrenebutanoic acid succinimidyl ester (1 mg/ml; Sigma-Aldrich) in methanol for 2 hours at room temperature, followed by cleaning with clean methanol. After that, the sensor was placed in GOD (10 mg/ml; Sigma-Aldrich) and CAT (2.0 mg/ml; Sigma-Aldrich) in deionized (DI) water for 18 hours at room temperature, rinsed with clean DI water, and then dried with nitrogen gas.

For the integration of glucose sensor with wireless display, the wireless display for the smart contact lens was delaminated from handling wafer by etching the Cu layer. Subsequently, the parylene layer was partially etched to integrate the electrodes and graphene channel. After that, the graphene channel was transferred to form the sensing channel, and embedding this wireless display sensor in the contact lens was conducted in the same manner as the embedding of the wireless display in the contact lens after the graphene channel was covered by the silaned polydimethylsiloxane mask. The immobilization procedure for the glucose sensor was identical with the above process.

### Rabbit experiments

All in vivo studies were conducted according to the guidelines of the National Institutes of Health for care and use of laboratory animals and with the approval of the Institute of Animal Care and Use Committee of the Ulsan National Institute of Science and Technology (UNIST) (UNISTIACUC-16-19). The Institute of Animal Care and Use Committee of UNIST was the ethics review committee. For the in vivo experiments, a male New Zealand white rabbit was used.

## SUPPLEMENTARY MATERIALS

Supplementary material for this article is available at http://advances.sciencemag.org/cgi/content/full/4/1/eaap9841/DC1

Supplementary Materials and Methods

fig. S1. Fabrication processing steps of the hybrid substrate.

fig. S2. AFM data analysis.

fig. S3. Optical transmittance (black) and haze (red) spectra of the silicone elastomeric film.

## REFERENCES AND NOTES

1. T. Yokota, P. Zalar, M. Kaltenbrunner, H. Jinno, N. Matsuhisa, H. Kitanosako, Y. Tachibana, W. Yukita, M. Koizumi, T. Someya, Ultraflexible organic photonic skin. *Sci. Adv.* **2**, e1501856 (2016).
2. B. C.-K. Tee, A. Chortos, A. Berndt, A. K. Nguyen, A. Tom, A. McGuire, Z. C. Lin, K. Tien, W.-G. Bae, H. Wang, P. Mei, H.-H. Chou, B. Cui, K. Deisseroth, T. N. Ng, Z. Bao, A skin-inspired organic digital mechanoreceptor. *Science* **350**, 313–316 (2015).
3. J. Kim, G. A. Salvatore, H. Araki, A. M. Chiarelli, Z. Xie, A. Banks, X. Sheng, Y. Liu, J. W. Lee, K.-I. Jang, S. Y. Heo, K. Cho, H. Luo, B. Zimmerman, J. Kim, L. Yan, X. Feng, S. Xu, M. Fabiani, G. Gratton, Y. Huang, U. Paik, J. A. Rogers, Battery-free, stretchable optoelectronic systems for wireless optical characterization of the skin. *Sci. Adv.* **2**, e1600418 (2016).
4. S. I. Park, D. S. Brenner, G. Shin, C. D. Morgan, B. A. Copits, H. U. Chung, M. Y. Pullen, K. N. Noh, S. Davidson, S. J. Oh, J. Yoon, K.-I. Jang, V. K. Samineni, M. Norman, J. G. Grajales-Reyes, S. K. Vogt, S. S. Sundaram, K. M. Wilson, J. S. Ha, R. Xu, T. Pan, T.-i. Kim, Y. Huang, M. C. Montana, J. P. Golden, M. R. Bruchas, R. W. Gereau IV, J. A. Rogers, Soft, stretchable, fully implantable miniaturized optoelectronic systems for wireless optogenetics. *Nat. Biotechnol.* **33**, 1280–1286 (2015).
5. C. Wang, D. Hwang, Z. Yu, K. Takei, J. Park, T. Chen, B. Ma, A. Javey, User-interactive electronic skin for instantaneous pressure visualization. *Nat. Mater.* **12**, 899–904 (2013).
6. D.-H. Kim, J. Viventi, J. J. Amsden, J. Xiao, L. Vigeland, Y.-S. Kim, J. A. Blanco, B. Panilaitis, E. S. Frechette, D. Contreras, D. L. Kaplan, F. G. Omenetto, Y. Huang, K.-C. Hwang, M. R. Zakin, B. Litt, J. A. Rogers, Dissolvable films of silk fibroin for ultrathin conformal bio-integrated electronics. *Nat. Mater.* **9**, 511–517 (2010).
7. H. Chu, H. Jang, Y. Lee, Y. Chae, J.-H. Ahn, Conformal, graphene-based triboelectric nanogenerator for self-powered wearable electronics. *Nano Energy* **27**, 298–305 (2016).
8. D.-H. Kim, N. Lu, R. Ma, Y.-S. Kim, R.-H. Kim, S. Wang, J. Wu, S. M. Won, H. Tao, A. Islam, K. J. Yu, T.-i. Kim, R. Chowdhury, M. Ying, L. Xu, M. Li, H.-J. Chung, H. Keum, M. McCormick, P. Liu, Y.-W. Zhang, F. G. Omenetto, Y. Huang, T. Coleman, J. A. Rogers, Epidermal electronics. *Science* **333**, 838–843 (2011).
9. W. Gao, S. Emaminejad, H. Y. Y. Nyein, S. Challa, K. Chen, A. Peck, H. M. Fahad, H. Ota, H. Shiraki, D. Kiriya, D.-H. Lien, G. A. Brooks, R. W. Davis, A. Javey, Fully integrated wearable sensor arrays for multiplexed in situ perspiration analysis. *Nature* **529**, 509–514 (2016).
10. J. G. McCall, T.-i. Kim, G. Shin, X. Huang, Y. H. Jung, R. Al-Hasani, F. G. Omenetto, M. R. Bruchas, J. A. Rogers, Fabrication and application of flexible, multimodal light-emitting devices for wireless optogenetics. *Nat. Protoc.* **8**, 2413–2428 (2013).
11. K.-I. Jang, S. Y. Han, S. Xu, K. E. Mathewson, Y. Zhang, J.-W. Jeong, G.-T. Kim, R. C. Webb, J. W. Lee, T. J. Dawidczyk, R. H. Kim, Y. M. Song, W.-H. Yeo, S. Kim, H. Cheng, S. I. Rhee, J. Chung, B. Kim, H. U. Chung, D. Lee, Y. Yang, M. Cho, J. G. Gaspar, R. Carbonari, M. Fabiani, G. Gratton, Y. Huang, J. A. Rogers, Rugged and breathable forms of stretchable electronics with adherent composite substrates for transcutaneous monitoring. *Nat. Commun.* **5**, 4779 (2014).
12. D. Kim, D. Kim, H. Lee, Y. R. Jeong, S.-J. Lee, G. Yang, H. Kim, G. Lee, S. Jeon, G. Zi, J. Kim, J. S. Ha, Body-attachable and stretchable multisensors integrated with wirelessly rechargeable energy storage devices. *Adv. Mater.* **28**, 748–756 (2016).
13. N. M. Farandos, A. K. Yetisen, M. J. Monteiro, C. R. Lowe, S. H. Yun, Contact lens sensors in ocular diagnostics. *Adv. Healthc. Mater.* **4**, 792–810 (2015).
14. J. Kim, M. Kim, M.-S. Lee, K. Kim, S. Ji, Y.-T. Kim, J. Park, K. Na, K.-H. Bae, H. K. Kim, F. Bien, C. Y. Lee, J.-U. Park, Wearable smart sensor systems integrated on soft contact lenses for wireless ocular diagnostics. *Nat. Commun.* **8**, 14997 (2017).
15. M. X. Chu, K. Miyajima, D. Takahashi, T. Arakawa, K. Sano, S.-i. Sawada, H. Kudo, Y. Iwasaki, K. Akiyoshi, M. Mochizuki, K. Mitsubayashi, Soft contact lens biosensor for in situ monitoring of tear glucose as non-invasive blood sugar assessment. *Talanta* **83**, 960–965 (2011).
16. H. Yao, A. J. Shum, M. Cowan, I. Lähdesmäki, B. A. Parviz, A contact lens with embedded sensor for monitoring tear glucose level. *Biosens. Bioelectron.* **26**, 3290–3296 (2011).
17. A. R. Lingley, M. Ali, Y. Liao, R. Mirjalili, M. Klonner, M. Sopanen, S. Suihkonen, T. Shen, B. P. Otis, H. Lipsanen, B. A. Parviz, A single-pixel wireless contact lens display. *J. Micromech. Microeng.* **21**, 125014 (2011).
18. G.-Z. Chen, I.-S. Chan, D. C. C. Lam, Capacitive contact lens sensor for continuous non-invasive intraocular pressure monitoring. *Sens. Actuators A Phys.* **203**, 112–118 (2013).
19. S. De Smedt, Noninvasive intraocular pressure monitoring: Current insights. *Clin. Ophthalmol.* **9**, 1385–1392 (2015).
20. Y.-T. Liao, H. Yao, A. Lingley, B. Parviz, B. P. Otis, A 3-μW CMOS glucose sensor for wireless contact-lens tear glucose monitoring. *IEEE J. Solid-State Circuits* **47**, 335–344 (2012).
21. D. Piso, P. Veiga-Crespo, E. Vecino, Modern monitoring intraocular pressure sensing devices based on application specific integrated circuits. *J. Biomater. Nanobiotechnol.* **3**, 301–309 (2012).
22. J. Pandey, Y.-T. Liao, A. Lingley, R. Mirjalili, B. Parviz, B. P. Otis, A fully integrated RF-powered contact lens with a single element display. *IEEE Trans. Biomed. Circuits Syst.* **4**, 454–461 (2010).
23. M. Leonardi, P. Leuenberger, D. Bertrand, A. Bertsch, P. Renaud, First steps toward noninvasive intraocular pressure monitoring with a sensing contact lens. *Invest. Ophthalmol. Vis. Sci.* **45**, 3113–3117 (2004).
24. I. M. Graz, D. P. J. Cotton, A. Robinson, S. P. Lacour, Silicone substrate with in situ strain relief for stretchable thin-film transistors. *Appl. Phys. Lett.* **98**, 124101 (2011).
25. R. M. Erb, K. H. Cherenack, R. E. Stahel, R. Libanori, T. Kinkeldei, N. Münzenrieder, G. Tröster, A. R. Studart, Locally reinforced polymer-based composites for elastic electronics. *ACS Appl. Mater. Interfaces* **4**, 2860–2864 (2012).
26. M. Kim, J. Park, S. Ji, S.-H. Shin, S.-Y. Kim, Y.-C. Kim, J.-Y. Kim, J.-U. Park, Fully-integrated, bezel-less transistor arrays using reversibly foldable interconnects and stretchable origami substrates. *Nanoscale* **8**, 9504–9510 (2016).
27. A. Romeo, Q. Liu, Z. Suo, S. P. Lacour, Elastomeric substrates with embedded stiff platforms for stretchable electronics. *Appl. Phys. Lett.* **102**, 131904 (2013).
28. S. Ji, B. G. Hyun, K. Kim, S. Y. Lee, S.-H. Kim, J.-Y. Kim, M. H. Song, J.-U. Park, Photo-patternable and transparent films using cellulose nanofibers for stretchable origami electronics. *NPG Asia Mater.* **8**, e299 (2016).
29. R. Libanori, R. M. Erb, A. Reiser, H. Le Ferrand, M. J. Süess, R. Spolenak, A. R. Studart, Stretchable heterogeneous composites with extreme mechanical gradients. *Nat. Commun.* **3**, 1265 (2012).
30. M.-S. Lee, K. Lee, S.-Y. Kim, H. Lee, J. Park, K.-H. Choi, H.-K. Kim, D.-G. Kim, D.-Y. Lee, S. Nam, J.-U. Park, High-performance, transparent, and stretchable electrodes using graphene–metal nanowire hybrid structures. *Nano Lett.* **13**, 2814–2821 (2013).
31. B. W. An, B. G. Hyun, S.-Y. Kim, M. Kim, M.-S. Lee, K. Lee, J. B. Koo, H. Y. Chu, B.-S. Bae, J.-U. Park, Stretchable and transparent electrodes using hybrid structures of graphene–metal nanotrough networks with high performances and ultimate uniformity. *Nano Lett.* **14**, 6322–6328 (2014).
32. J. Kim, M.-S. Lee, S. Jeon, M. Kim, S. Kim, K. Kim, F. Bien, S. Y. Hong, J.-U. Park, Highly transparent and stretchable field-effect transistor sensors using graphene–nanowire hybrid nanostructures. *Adv. Mater.* **27**, 3292–3297 (2015).
33. J. Jang, B. G. Hyun, S. Ji, E. Cho, B. W. An, W. H. Cheong, J.-U. Park, Rapid production of large-area, transparent and stretchable electrodes using metal nanofibers as wirelessly operated wearable heaters. *NPG Asia Mater.* **9**, e432 (2017).
34. H. G. Craighead, J. Cheng, S. Hackwood, New display based on electrically induced index-matching in an inhomogeneous medium. *Appl. Phys. Lett.* **40**, 22–24 (1982).
35. K. Besteman, J.-O. Lee, F. G. M. Wiertz, H. A. Heering, C. Dekker, Enzyme-coated carbon nanotubes as single-molecule biosensors. *Nano Lett.* **3**, 727–730 (2003).
36. R. J. Chen, Y. Zhang, D. Wang, H. Dai, Noncovalent sidewall functionalization of single-walled carbon nanotubes for protein immobilization. *J. Am. Chem. Soc.* **123**, 3838–3839 (2001).
37. J. Liu, M. Agarwal, K. Varahramyan, Glucose sensor based on organic thin film transistor using glucose oxidase and conducting polymer. *Sens. Actuators B Chem.* **135**, 195–199 (2008).
38. M. Ngoepe, Y. E. Choonara, C. Tyagi, L. K. Tomar, L. C. du Toit, P. Kumar, V. M. K. Ndesendo, V. Pillay, Integration of biosensors and drug delivery technologies for early detection and chronic management of illness. *Sensors* **13**, 7680–7713 (2013).
39. S. Singh, M. McShane, Enhancing the longevity of microparticle-based glucose sensors towards 1 month continuous operation. *Biosens. Bioelectron.* **25**, 1075–1081 (2010).
40. D. K. Sen, G. S. Sarin, Tear glucose levels in normal people and in diabetic patients. *Br. J. Ophthalmol.* **64**, 693–695 (1980).
41. D. C. Rodger, J. D. Weiland, M. S. Humayun, Y.-C. Tai, Scalable high lead-count parylene package for retinal prostheses. *Sens. Actuators B Chem.* **117**, 107–114 (2006).

42. IEEE, IEEE standard for safety levels with respect to human exposure to radio frequency electromagnetic fields, 3 kHz to 300 GHz, in *IEEE Std C951-2005 (Revision of IEEE Std C951-1991)* (IEEE, 2006), 238 pp.
43. H. Lee, T. K. Choi, Y. B. Lee, H. R. Cho, R. Ghaffari, L. Wang, H. J. Choi, T. D. Chung, N. Lu, T. Hyeon, S. H. Choi, D.-H. Kim, A graphene-based electrochemical device with thermoresponsive microneedles for diabetes monitoring and therapy. *Nat. Nanotechnol.* **11**, 566–572 (2016).
44. A. Koh, D. Kang, Y. Xue, S. Lee, R. M. Pielak, J. Kim, T. Hwang, S. Min, A. Banks, P. Bastien, M. C. Manco, L. Wang, K. R. Ammann, K.-I. Jang, P. Won, S. Han, R. Ghaffari, U. Paik, M. J. Slepian, G. Balooch, Y. Huang, J. A. Rogers, A soft, wearable microfluidic device for the capture, storage, and colorimetric sensing of sweat. *Sci. Transl. Med.* **8**, 366ra165 (2016).
45. T. Arakawa, Y. Kuroki, H. Nitta, P. Chouhan, K. Toma, S.-i. Sawada, S. Takeuchi, T. Sekita, K. Akiyoshi, S. Minakuchi, K. Mitsubayashi, Mouthguard biosensor with telemetry system for monitoring of saliva glucose: A novel *cavitas* sensor. *Biosens. Bioelectron.* **84**, 106–111 (2016).

**Acknowledgments**
**Funding:** This work was supported by the Ministry of Science and ICT and the Ministry of Trade, Industry and Energy of Korea through the National Research Foundation (2016R1A2B3013592 and 2016R1A5A1009926), the Nano-Material Technology Development Program (2015M3A7B4050308 and 2016M3A7B4910635), the Convergence Technology Development Program for Bionic Arm (NRF-2017M3C1B2085316), the Industrial Technology Innovation Program (10080577), and the Pioneer Research Center Program (NRF-2014M3C1A3001208). Also, the authors thank CooperVision Awards and acknowledge financial support by the Development Program (1.170009.01) funded by UNIST. **Author contributions:** J.P., J.K., and S.-Y.K. carried out the experiments, analyzed the data, and wrote the manuscript. W.H.C., J.J., Y.-G.P., K.N., Y.-T.K., and J.H.H. performed the experiments. C.Y.L. contributed to the project planning. J.H.L., F.B., and J.-U.P. oversaw all the research phases and revised the manuscript. All authors discussed and commented on the manuscript. **Competing interests:** All authors declare that they have no competing interests. **Data and materials availability:** All data needed to evaluate the conclusions in the paper are present in the paper and/or the Supplementary Materials. Additional data related to this paper may be requested from the authors.

Submitted 17 September 2017
Accepted 14 December 2017
Published 24 January 2018
10.1126/sciadv.aap9841

**Citation:** J. Park, J. Kim, S.-Y. Kim, W. H. Cheong, J. Jang, Y.-G. Park, K. Na, Y.-T. Kim, J. H. Heo, C. Y. Lee, J. H. Lee, F. Bien, J.-U. Park, Soft, smart contact lenses with integrations of wireless circuits, glucose sensors, and displays. *Sci. Adv.* **4**, eaap9841 (2018).

ScienceAdvances

# Soft, smart contact lenses with integrations of wireless circuits, glucose sensors, and displays

Jihun Park, Joohee Kim, So-Yun Kim, Woon Hyung Cheong, Jiuk Jang, Young-Geun Park, Kyungmin Na, Yun-Tae Kim, Jun Hyuk Heo, Chang Young Lee, Jung Heon Lee, Franklin Bien and Jang-Ung Park

*Sci Adv* **4** (1), eaap9841.
DOI: 10.1126/sciadv.aap9841